Differential Capacity of Bromide Anions Adsorption onto Ag(100) in the Absence, and onto Ag(poly) in the Presence of NaClO₄

V. D. Jović

Institute for Multidisciplinary Research,
11030 Belgrade, P. O. Box 33, Serbia
e-mail: vladajovic@ibiss.bg.ac.yu

In this work, the adsorption of bromide anions onto Ag(100) and Ag(poly) in the absence and presence of NaClO₄ was investigated. The cyclic voltammetry, EIS and C_{diff} vs. E measurement results were analyzed. For the determination of the adsorption parameters, the equivalent circuit containing constant phase element (*CPE*) instead of the double layer capacity (C_{dl}) and new equations for the analysis of the anion adsorption, based on a different definition of the *CPE*, have been developed and used. It was shown that the proposed equivalent circuit and corresponding equations for the differential capacity (C_{diff}) as a function of frequency (ω) can successfully be applied in the investigated systems. Excellent agreement between the cyclic voltammograms (CVs) and the C_{diff} vs. E curves recorded at frequencies lower than 10 Hz has been detected. The homogeneity of the charge distribution over the real single crystal surfaces, as well as other parameters of the adsorption process were found to change with the potential. In the presence of the supporting ("non-adsorbing") electrolyte (0.1 M NaClO₄) diffusion-like phenomenon was detected and ascribed to the slow step in exchanging anions adsorbed in the inner Helmholtz plane.

Key words:
Bromide anions adsorption, differential capacity, CPE, surface homogeneity

Introduction

The determination of the double layer capacities in the available literature is, so far, mainly based on either differential capacity measurements (C_{diff} vs. E curves) performed at a single frequency,[1–6] or on impedance measurements performed in a broad range of frequencies and the analysis of impedance diagrams using the adsorption impedance theory developed by M. Sluyters-Rehbach *et al.*[7] Using equations for the impedance and capacitance defined by this theory[7,8] the equation for the differential capacity is defined as

$$C_{diff} = Y_{Im}^{corr} \omega^{-1} =$$
$$= C_{dl} + \frac{C_{ad}(1 + \omega^{1/2} C_{ad} \sigma)}{(1 + \omega^{1/2} C_{ad} \sigma)^2 + \omega^2 C_{ad}^2 (R_{ad} + \omega^{-1/2} \sigma)^2} \quad (1)$$

where Y_{Im}^{corr} represents imaginary component of admittance corrected for R_s, ω is the angular frequency ($\omega = 2\pi f$, f being the frequency), R_s represents resistance of the solution, C_{dl} the double layer capacity, while C_{ad}, R_{ad} and σ correspond to the capacity, resistance and the Warburg coefficient of the anion adsorption, respectively. It should be noted that in order to obtain the real value for the C_{dl}, solution resistance (R_s) must be subtracted from the total electrode impedance (Y_{Im}^{corr} in the eq. (1)).

Taking into account that the Warburg coefficient of the anion adsorption (σ) depends on the concentration (c) and the diffusion coefficient (D) of adsorbing anions, it could be concluded from the eq. (1) that at high frequencies and low concentrations of adsorbing anions, the contribution of the second term in this equation becomes insignificant and the C_{diff} vs. f corresponds to the double layer capacity only. Using the values for $C_{dl} = 60$ μF cm⁻², $C_{ad} = 200$ μF cm², $R_{ad} = 50$ Ω cm², $D = 1 \cdot 10^{-5}$ cm² s⁻¹ and varying the value of c from 100 mM to 0.01 mM in eq. (1), C_{diff} vs. f diagrams presented in Fig. 1 were obtained. As can be seen, for higher concentrations of anions (1, 10 and 100 mM) their diffusion has no influence on the shape of the C_{diff} vs. f curves. The total capacitance is independent of frequency and equal to C_{dl} at $f > 10^2$ Hz (point A), while at $f < 10^0$ Hz, the total capacitance is also independent of frequency and equal to the sum $C_{dl} + C_{ad}$ (point B). At lower concentrations (0.1 and 0.01 mM), the differential capacity is again independent of frequency and equal to C_{dl} at $f > 10^2$ Hz (point A), while C_{diff} depends on frequency at frequencies lower than 10^2 Hz, as a consequence of the anion diffusion, and does not represent the sum $C_{dl} + C_{ad}$ (its value cannot reach the sum of $C_{dl} + C_{ad}$ even at $f = 10^{-4}$ Hz). This indicates that the real value of the C_{ad} (independent of frequency)
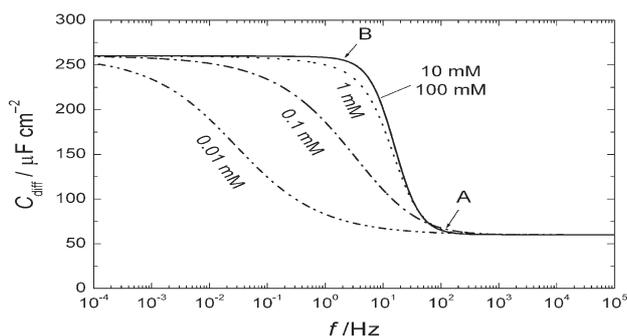
F i g . 1 – *Calculated C_{diff} vs. f curves for the adsorption of anions defined by eq. (1) for the following parameter values: $R_{ad} = 50\ \Omega\ cm^2$; $C_{dl} = 60\ \mu F\ cm^{-2}$; $C_{ad} = 200\ \mu F\ cm^{-2}$; $D = 1 \cdot 10^{-5}\ cm^2\ s^{-1}$. The concentrations of anions (c) are marked in the figure.*

cannot be determined from the C_{diff} vs. f curves for these concentrations of anions. It is important to note that most of the experiments concerning C_{diff} vs. E curves were performed in the solutions of investigated anion concentrations lower than 100 mM, usually of the order of 1 mM in the frequency range between 10 and 20 Hz,[5,6] exactly in the region of frequencies where C_{diff} increases sharply with decreasing the frequency (frequency region between A and B). In order to decrease the solution resistance in almost all cases a supporting ("non-adsorbing" – mostly perchlorate) electrolyte was added to the solution.

All the above mentioned consideration is valid for the systems where the double layer capacity behaves as an "ideal double layer", i.e. assuming homogeneous electrode surfaces (homogeneous charge distribution over the surface) and the double layer capacity being represented by a parallel plate condenser.[1–8] The introduction of the constant phase element (*CPE*) instead of the double layer capacity is also discussed in the literature.[9–24] Several phenomena, such as distributed surface reactivity, surface heterogeneity, roughness or fractal geometry, electrode porosity and current and potential distribution associated with electrode geometry were attributed to the *CPE* behavior in the literature.[9–24] The different expressions given for the *CPE* indicates that its physical meaning is not yet clear.

A recent experimental study of Kerner *et al.*[25] showed that capacitance dispersion on solid electrodes was due to surface disorder (i.e. heterogeneities on the atomic scale) rather than roughness (i.e. geometric irregularities much larger than those on the atomic scale). Kim *et al.*[26] also showed that the contribution of surface heterogeneity can be much higher than the contribution of the surface irregularity to the capacitance dispersion.

Most recently M. Orazem *et al.*[27] discussed different procedures for the treatment of the distribu-

tion of time constants and pointed out that the impedance of an equivalent circuit for parallel connection of *CPE* and resistance (*R*) can be expressed by two different equations

$$Z(\omega) = \frac{R}{1 + (j\omega CR)^{\alpha}} \tag{2}$$

and

$$Z(\omega) = \frac{R}{1 + (j\omega)^{\alpha} CR} \tag{3}$$

It is important to note that eq. (3) was used in all commercially available software for fitting impedance spectra, as well as in our previous paper.[28] In such a case *CPE* was considered as an independent element of the equivalent circuit and its impedance[29,30] was defined as $Z_{CPE} = 1/[Y_0(j\omega)^{\alpha}]$, while the values of Y_0 and α were obtained by fitting procedure, with the constant Y_0 having dimension $\Omega^{-1}cm^{-2}s^{\alpha}$. Accordingly, its value should be corrected by the procedure defined in the paper of Hsu *et al.*[31] in order to obtain correct dimension for the capacity, by following equation

$$C = Y_0(\omega_{Im}^{max})^{\alpha-1} \tag{4}$$

with ω_{Im}^{max} being the frequency of the maximum on $-Z_{Im}$ vs. log ω dependence, independent of the value of α. Eq. (4) is a result of the application of eq. (2) in the case of the analysis of the equivalent circuit with the parallel connection between *CPE* and *R*. If the value of ω_{Im}^{max} cannot be determined (in the case where the maximum on $-Z_{Im}$ vs. log ω dependence, i.e. the maximum on the semi-circle of the complex plane Z_{Im} vs. Z_{Re} does not exist, which is almost always the case on these diagrams obtained for anion adsorption, the real (dimensionally correct) value of the capacity cannot also be determined. In such a case the following equation should be used.

$$C = [Y_0(R)^{1-\alpha}]^{1/\alpha} \tag{5}$$

Eqs. (2), (4) and (5) assume that both parameters, C and R depend on α in the same way. The frequency dispersion of the capacity as a consequence of the surface heterogeneity (expressed as α) is closely related to the charge distribution over the same surface and these two parameters are mutually dependent. Such a statement is also pointed out by Van Meirhaege[32] in the analysis of the capacity of semiconductors.[33] According to these two references, "the frequency dependence of the capacity must be accompanied by a frequency-dependent parallel resistance".

The model and the equivalent circuit for anion adsorption onto real single crystals

After the in situ STM technique is introduced in the processes of the double layer and anion adsorption investigation onto single crystal surfaces,[34] it was obvious that even single crystal surfaces are not perfectly flat, but to the contrary, it is shown that they consist preferentially of a significant number of atomically flat terraces separated by monoatomic steps (for the best surface).[34–45] A typical example is demonstrated in Fig. 1 of Ref. 35, showing not only monoatomic steps, but also the presence of much more pronounced irregularities on the real single crystal surfaces of Ag(111) and Ag(100). It is also shown that during the process of anion adsorption, the first step is adsorption of anions at the monoatomic steps accompanied by the dynamic change of the STM image and movement of the monoatomic steps and terraces along the electrode surface,[37–42] indicating the presence of heterogeneous charge distribution over the single crystal surface. Simultaneously with the adsorption of anions at the monoatomic steps, adsorption of anions also takes place at the flat terraces with a formation of 2D islands of (most probably ordered) adsorbed structures (homogeneous charge transfer distribution over the terrace), while the movement of monoatomic steps and terraces along the electrode surface still occurs.[37–42] After reaching the potentials of the sharp peaks on the CVs, in all cases ordered adsorbed structures were detected all over the electrode surface and the movement of monoatomic steps and terraces was not so pronounced.[34–45] Hence, in such a case it would be reasonable to assume that these two processes, the adsorption on the heterogeneous and the homogeneous part of the electrode surface, occur simultaneously during the anion adsorption in a certain potential region.

In our previous papers, it was shown for the Ag(111) in 0.01 M NaCl[28] and Cu single crystals in 0.1 M NaOH[46] that C_{diff} vs. E curves are very sensitive to the frequency although the process of anion adsorption is not controlled by anion diffusion, indicating that even single crystal surfaces cannot be treated as being homogeneous and that, instead of C_{dl}, a *CPE* should be introduced in the analysis of C_{diff} vs. ω curves.

Accordingly, considering all above mentioned, it could be concluded that the equivalent circuit for the anion adsorption onto real single crystal surfaces should be represented by the one shown in Fig. 2, with $R_{\mathrm{ad}}^{\mathrm{he}}$ and $CPE_{\mathrm{dl}}^{\mathrm{he}}$ corresponding to the adsorption resistance and constant phase element on the heterogeneous part of the surface respectively (practically the inner Helmholtz layer, including the outer Helmholtz layer on the whole surface) and
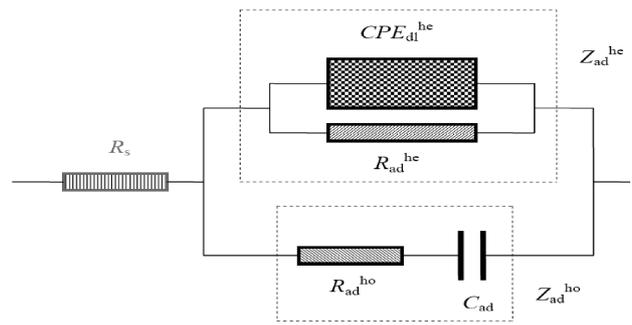
F i g . 2 – *Equivalent circuit for the anion adsorption onto real single crystal surfaces: R_s – solution resistance; R_{ad}^{he} – charge transfer resistance corresponding to the adsorption of anions on the heterogeneous part of the surface; CPE_{dl}^{he} – constant phase element corresponding to the adsorption of anions on the heterogeneous part of the surface; R_{ad}^{ho} – charge transfer resistance corresponding to the adsorption of anions on the homogeneous part of the surface; C_{ad} – capacitance corresponding to the adsorption of anions onto homogeneous part of the surface.*

$R_{\mathrm{ad}}^{\mathrm{ho}}$ and C_{ad} corresponding to the adsorption resistance and capacity on the homogeneous part of the surface respectively. By analysis of the equivalent circuit presented in Fig. 2, the following equation was obtained for the C_{diff} (after subtraction of the solution resistance, R_{s}, as in eq. (1)):

$$Y_{\mathrm{lm}}\omega^{-1} \equiv C_{\mathrm{diff}} = (C_{\mathrm{dl}})^{\alpha}(\omega R_{\mathrm{ad}}^{\mathrm{he}})^{\alpha-1}\sin\left(\frac{\alpha\pi}{2}\right) +$$
$$+ \frac{C_{\mathrm{ad}}}{1+\omega^2(C_{\mathrm{ad}})^2(R_{\mathrm{ad}}^{\mathrm{ho}})^2} \qquad (6)$$

Using the values for $C_{\mathrm{dl}} = 60$ µF cm^{-2}, $C_{\mathrm{ad}} = 200$ µF cm^{-2}, $R_{\mathrm{ad}}^{\mathrm{ho}} = 50$ Ω cm^2 and $R_{\mathrm{ad}}^{\mathrm{he}} = 5000$ Ω cm^2 and varying the value of α from 1.00 to 0.80, the diagrams presented in Fig. 3a were obtained. As can be seen, this dependence is very sensitive to the value of α (as well as to the other parameters) in a whole range of frequencies, being characterized by two inflection points (marked in the figure as A and B, as in the case of Fig. 1). In the range of high frequencies ($f > 10^2$ Hz for given equivalent circuit parameters) C_{diff} slightly changes with f down to the inflection point A for all values $\alpha < 1$. Between the inflection points A and B sharp, a non-linear increase of C_{diff} with f occurs, while with further decrease of frequency C_{diff} exponentially increases, with this increase being more pronounced at lower values of α. The values of C_{diff} at inflection points are defined by the values of C_{dl} (A) and $C_{\mathrm{ad}} + C_{\mathrm{dl}}$ (B). The position of the inflection points on the frequency axis (not shown in this work) is also sensitive to the values of the resistances $R_{\mathrm{ad}}^{\mathrm{ho}}$ and $R_{\mathrm{ad}}^{\mathrm{he}}$. It should be noted here that eq. (6) is dimensionally correct, i.e. its dimension is capacitance per unit area. Hence, it could be concluded that if C_{diff} vs. f function is dependent on frequency in the whole

range of applied frequencies, α is lower than 1 and, accordingly, C_{dl} should be replaced with *CPE* in the equivalent circuit.

For the results presented in Fig. 3a it was assumed that the adsorption process was under activation control (higher concentration of anions than 1 mM). If the diffusion, represented by the Warburg impedance, was introduced in the equivalent circuit (in series with C_{ad} and R_{ad}^{ho}), the following equation for the C_{diff} vs. ω was obtained.

$$C_{diff} = (C_{dl})^{\alpha}(\omega R_{ad}^{he})^{\alpha-1}\sin\left(\frac{\alpha\pi}{2}\right) + $$
$$+ \frac{C_{ad}(1 + \omega^{1/2}C_{ad}\sigma)}{(1 + \omega^{1/2}C_{ad}\sigma)^2 + \omega^2 C_{ad}^2(R_{ad}^{ho} + \omega^{-1/2}\sigma)^2} \quad (7)$$
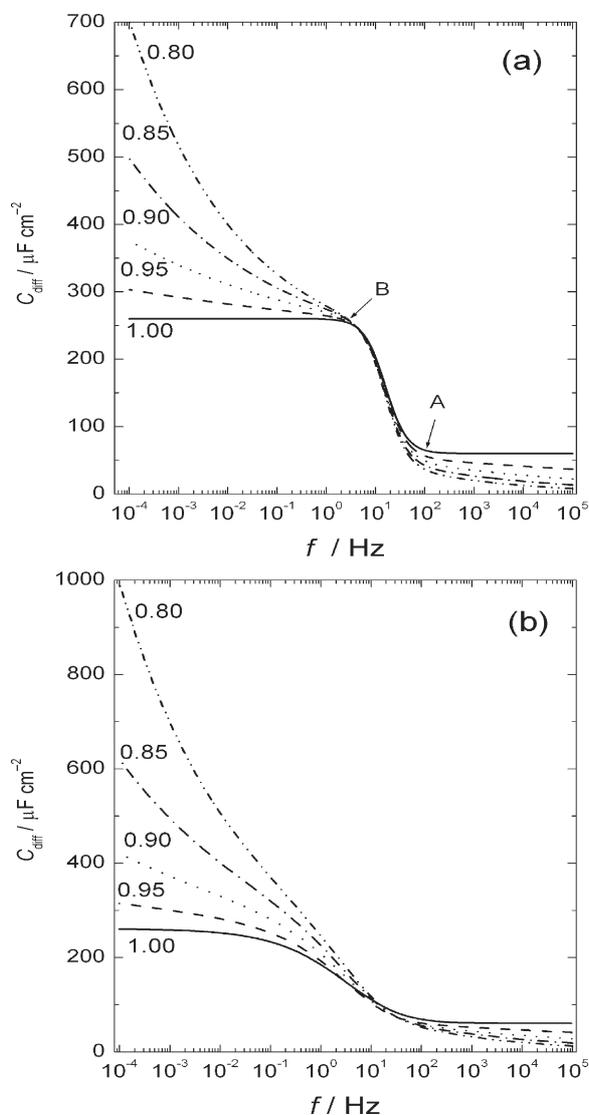
F i g . 3 – *(a) C_{diff} vs. f curves calculated using eq. (6): R_{ad}^{ho} = 50 Ω cm²; R_{ad}^{he} = 5000 Ω cm²; C_{dl} = 60 μF cm⁻²; C_{ad} = 200 μF cm⁻². The values of α are marked in the figure. (b) C_{diff} vs. f curves calculated using eq. (7): R_{ad}^{ho} = 50 Ω cm²; R_{ad}^{he} = 5000 Ω cm²; C_{dl} = 60 μF cm⁻²; C_{ad} = 200 μF cm⁻²; c = 0.1 mM. The values of α are marked in the figure.*

Using the same parameter values as in Fig. 3a for the concentration (*c*) of 0.1 mM, the C_{diff} vs. *f* dependences shown in Fig. 3b were obtained. As can be seen, inflection points A and B are defined only for α = 1, while for all other values of α practically exponential dependence is obtained in the whole range of frequencies. Hence, if the diffusion phenomena are involved and the charge distribution is not homogeneous, it is practically impossible to determine the values of the adsorption parameters by plotting C_{diff} vs. *E* curve for a single frequency.

In this paper, the dependences of the C_{diff} vs. ω, as well as C_{diff} vs. *E* for the systems Ag(100)/0.01 M NaBr and Ag(poly)/0.01 M NaBr + 0.1 M NaClO₄, using the above-mentioned approach, were analyzed and discussed.

Experimental

All experiments were carried out in a two-compartment electrochemical cell at the temperature of 25 ± 1 °C. The single crystal and polycrystalline electrodes (Monocrystals Company, *d* = 0.9 cm) were sealed in an epoxy resin (resin EPON 828 + hardener TETA) in such a way that only the disc surfaces were exposed to the solution (0.636 cm²). The counter electrode was a Pt sheet and was placed parallel to the working electrode surface. The reference electrode was a saturated calomel electrode (SCE) placed in a separate compartment and connected to the working compartment by means of a Luggin capillary. Solutions were made from pure NaBr (99.999 % – Aldrich) and NaClO₄ (99.98 % – Aldrich) chemicals and extra pure UV water (Smart2PureUV, TKA). All potentials are given vs. SCE.

The single and polycrystalline surfaces were prepared by a mechanical polishing procedure followed by chemical polishing in the solution containing NaCN and H₂O₂ as explained in detail in previous papers.[28,46,47,62–65] Before each experiment, the electrolyte was purged with high purity nitrogen (99.999 %) for 45 min, while a nitrogen atmosphere was maintained over the solution during the experiment to prevent contamination with oxygen.

The cyclic voltammetry experiments were performed using a universal programmer PAR M-175, a potentiostat PAR M-173 and an X-Y recorder (Houston Instrument 2000R). A potentiostat Reference 600 and a software EIS300 – version 5.0 (Gamry Instruments) were used to perform EIS and differential capacity measurements with an amplitude of 10 mV.

The differential capacity vs. potential curves for the system Ag(100)/0.01 M NaBr were obtained by the following procedure: Potential of the electrode was changed in steps of 50 mV starting from –1.2 V and finishing at – 0.1 V; at each applied potential the values of the real and imaginary components of the impedance were recorded at different frequencies (1000, 700, 400, 200, 100, 70, 40, 20, 10, 7, 4, 2, 1, 0.7, 0.4, 0.2 and 0.1 Hz); these values were corrected for the solution resistance R_s (determined from the high frequency intercept on the Z_{Re} axis of Z_{Im} vs. Z_{Re} diagrams, see Figs. 5 and 9) and converted into C_{diff}. For each potential the C_{diff} vs. ω curves were plotted. The EIS measurements at three different potentials were performed in the frequency range from 0.01 Hz to 10 kHz with 10 points per decade and the same amplitude. Fitting of C_{diff} vs. ω curves was performed using the commercially available Origin 6.1 program. One of the most powerful and complex components of the Origin program is its nonlinear least squares fitting (NLSF) capability. Its nonlinear regression method is based on the Levenberg-Marquardt (LM) algorithm and is the most widely used algorithm in nonlinear least squares fitting. The NLSF always reported the reduced chi^2 value, varying from $1.02 \cdot 10^{-12}$ to $6.07 \cdot 10^{-15}$, as well as the coefficient of determination (R^2), varying from 0.99748 to 0.99987 with "no weighting" function. The curves connecting experimental points presented in Figs. 4a, 5, 7, 8b, 9 and 11 were obtained by using B-spline function (smoothing the curve) defined in the Origin program.

In the case of the system Ag(poly)/0.01 M NaBr + 0.1 M NaClO$_4$, CV and EIS were recorded using the Gamry Reference 600 potentiostat. Instead of using the previously described procedure, the EIS measurements were performed at different potentials (in steps of 50 mV) from –1.0 V to –0.05 V (in the frequency range from 0.1 Hz to 10 kHz with the amplitude of 10 mV). For each potential, the C_{diff} vs. ω curves were plotted and analyzed by the same procedure as for the Ag(100)/0.01 M NaBr system (using Origin program). In order to plot C_{diff} vs. E curves, the C_{diff} values at certain frequencies (0.1, 1, 10 and 100 Hz) were used. It should be emphasized that the value of the differential capacity was calculated in all cases using the equation

$$C_{diff} = \frac{Y_{Im}^{corr}}{\omega} = \frac{\dfrac{Z_{Im}}{(Z_{Re} - R_s)^2 + (Z_{Im})^2}}{\omega} \quad (8)$$

Each experiment was repeated three times and the average values presented in this paper. The variation of the results was ± 5 %.

Results

System Ag(100)/0.01M NaBr

The CV recorded for the Ag(100) in 0.01 M NaBr solution at a sweep rate of 100 mV s^{-1} is shown in Fig. 4a. As can be seen, the voltammogram is in good agreement with the results of other authors,[48,49] being characterized by almost reversible pairs of broad and sharp peaks.

Fig. 5 shows the results of the EIS measurements performed for the same system at three constant potentials (frequencies are in Hz). The high frequency ends of the Z_{Im} vs. Z_{Re} diagrams are presented in the inset of the figure. The solution resistance was determined by linear extrapolation to the
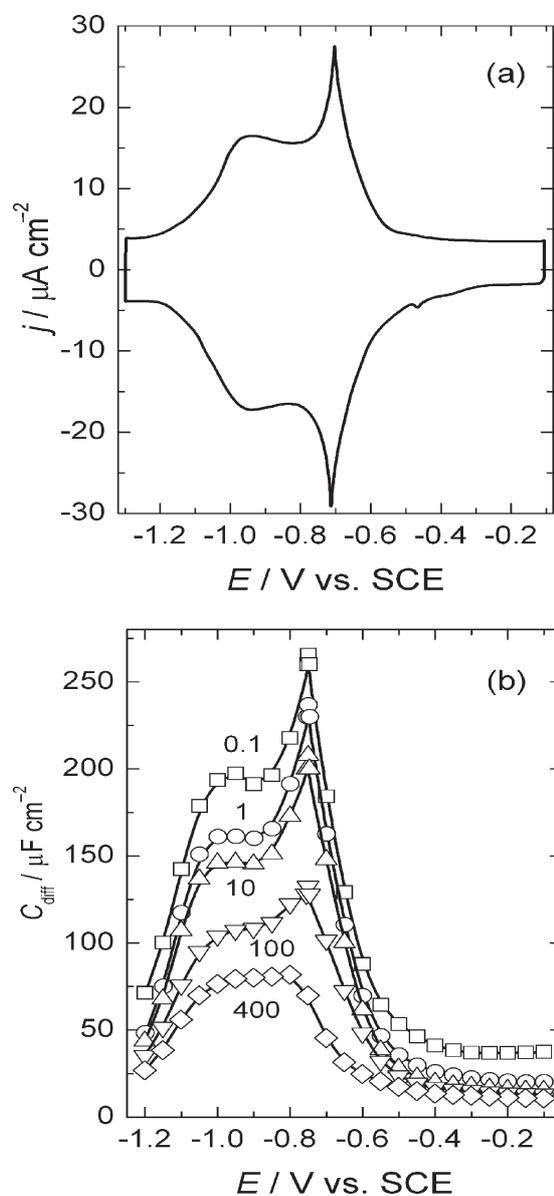
Fig. 4 – (a) CV of Ag(100) in 0.01 M NaBr recorded at a sweep rate of 100 mV s^{-1}. (b) Corresponding C_{diff} vs. E curves recorded at different frequencies (marked in the figure in Hz).
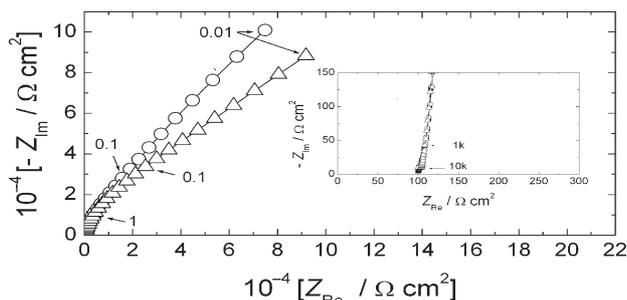
F i g .   5 – *Z_{Im} vs. Z_{Re} diagrams recorded at potentials of –1.10 V (■), –0.50 V (○) and –0.30 V (△) in the frequency range from 0.01 to 10000 Hz for the system Ag(100)/0.01 M NaBr. The high frequency ends of Z_{Im} vs. Z_{Re} diagrams, used for determination of R_s, are presented in the inset. Frequencies are marked in Hz.*

Z_{Re} axis, whereby the value $R_s = 102$ Ω cm² was obtained for all potentials. As can be seen, none of the impedance diagrams is even close to the shape typical for "ideal double layer behavior".

Some of the obtained C_{diff} vs. E curves are shown in Fig. 4b. The dispersion of points on the C_{diff} vs. E curves at the frequencies $f > 400$ Hz was significant and these results were not used for further analysis (at high frequencies the difference between the values of Z_{Re} and R_s is very small and, accordingly, the value of $Z_{Re}-R_s$ becomes very sensitive to the measured Z_{Re} and extrapolated R_s, producing dissipation of points on the C_{diff} vs. E curves). As can be seen, C_{diff} was found to depend on frequency in the whole range of investigated frequencies, as it was the case with Ag(111) in 0.01 M NaCl (Ref. 28, Fig. 5).

Using the values of C_{diff} at a constant potential (from the C_{diff} vs. E curves), C_{diff} vs. ω curves were plotted, some of which have been presented in Fig. 6. In order to obtain the values for C_{dl}, C_{ad}, R_{ad}^{ho}, R_{ad}^{he} and α, fitting of the C_{diff} vs. ω curves was performed using eq. (6), as explained in the experimental section. The experimental points are presented by squares, circles, triangles, etc., while the

lines represent the fitting curves. Potentials are marked in the figure for each curve. As can be seen, good fits were obtained with very high values of the coefficient of determination (R^2) (see experimental). Identical results were obtained for the rest of the C_{diff} vs. ω curves, not presented in Fig. 6.

The dependences of the parameters C_{dl}, C_{ad}, ($C_{dl} + C_{ad}$), R_{ad}^{ho}, R_{ad}^{he} and α on potential are shown in Fig. 7. As can be seen in Fig. 7a, only C_{ad} vs. E curve coincide well with the corresponding CV, whereas the value of α sharply decreases at the maximum on the C_{ad} vs. E (△) curve, indicating significant heterogeneity of the charge distribution over the electrode surface at potentials more positive than the potential of the sharp peak on the CV (Fig. 4a). Resulting R_{ad}^{ho} vs. E and R_{ad}^{he} vs. E dependences are also different, as shown in Fig. 7b.
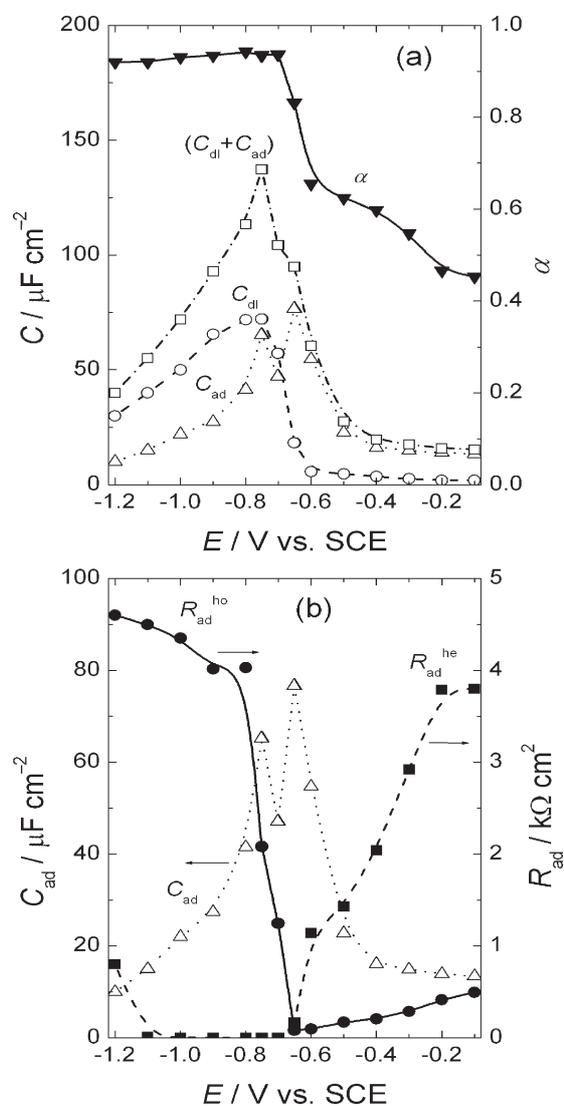
F i g .   7 – *Results obtained by fitting the C_{diff} vs. ω curves for different potentials with eq. (6) for the system Ag(100)/0.01 M NaBr; (a) C_{ad} vs. E (△), C_{dl} vs. E (○), ($C_{dl} + C_{ad}$) vs. E (□) and α vs. E (▼) curves. (b) C_{ad} vs. E (△), R_{ad}^{ho} vs. E (●) and R_{ad}^{he} vs. E (◆) curves.*

F i g .   6 – *C_{diff} vs. ω curves for different potentials (marked in the figure) obtained from the C_{diff} vs. E curves for the system Ag(100)/0.01 M NaBr. The squares, circles, triangles, etc. represent the experimental points, while the full lines represent the fitted curves obtained by using eq. (6).*

The charge recorded under the anodic part of the voltammogram shown in Fig. 4a, as well as the charges obtained by the integration of C_{dl} vs. E, C_{ad} vs. E and (C_{dl} + C_{ad}) vs. E curves presented in Fig. 7a are given in Table 1.

T a b l e 1 – *Charge recorded under corresponding curves for the system Ag(100)/0.01 M NaBr. Theoretical charge for c(2x2) = 96 μC cm^{-2}(assuming complete charge transfer).*

Curve	Charge
Anodic part of the CV	105 μC cm^{-2}
C_{ad} vs. E	31 μC cm^{-2}
C_{dl} vs. E	32 μC cm^{-2}
(C_{dl} + C_{ad}) vs. E	63 μC cm^{-2}

System Ag(poly)/0.01 M NaBr + 0.1 M NaClO$_4$

The CV recorded at the Ag(poly) in 0.01 M NaBr + 0.1 M NaClO$_4$ solution at a sweep rate of 100 mV s^{-1} is shown in Fig. 8a, while C_{diff} vs. E curves are shown in Fig. 8b (frequencies are in Hz). As can be seen, the CV is in good agreement with the C_{diff} vs. E curves recorded for low frequencies (< 10 Hz), particularly with the curve recorded for f = 0.1 Hz. The CV (as well as C_{diff} vs. E curves) is characterized with three different regions, double layer region (A) and adsorption regions (B) and (C). At the potentials close to zero, a "nucleation loop" reflecting formation of 3D layer of AgBr is detected.

Fig. 9 shows the EIS measurements performed for this system at four constant potentials. The high frequency ends of the Z_{Im} vs. Z_{Re} diagrams are presented in the inset of the figure. The solution resistance was determined by linear extrapolation to the Z_{Re} axis, whereby the value R_s = 8.16 Ω cm^2 was obtained for all potentials. As in a previous case, none of the impedance diagrams is even close to the shape typical for "ideal double layer behavior".

Some of the C_{diff} vs. ω curves were plotted in Fig. 10. As can be seen, the shape of these curves depends on the potential regions, being sensitive to the potential in the regions (A) and (B), and practically insensitive to the potential in the region (C). In order to obtain values for C_{dl}, C_{ad}, R_{ad}^{ho}, R_{ad}^{he}, σ and α, fitting of the C_{diff} vs. ω curves was performed using eq. (7) since the use of eq. (6) could not give good results (see discussion). The experimental points are presented by squares, circles, triangles, etc., while the lines represent the fitting curves. Potentials are marked in the figure for each
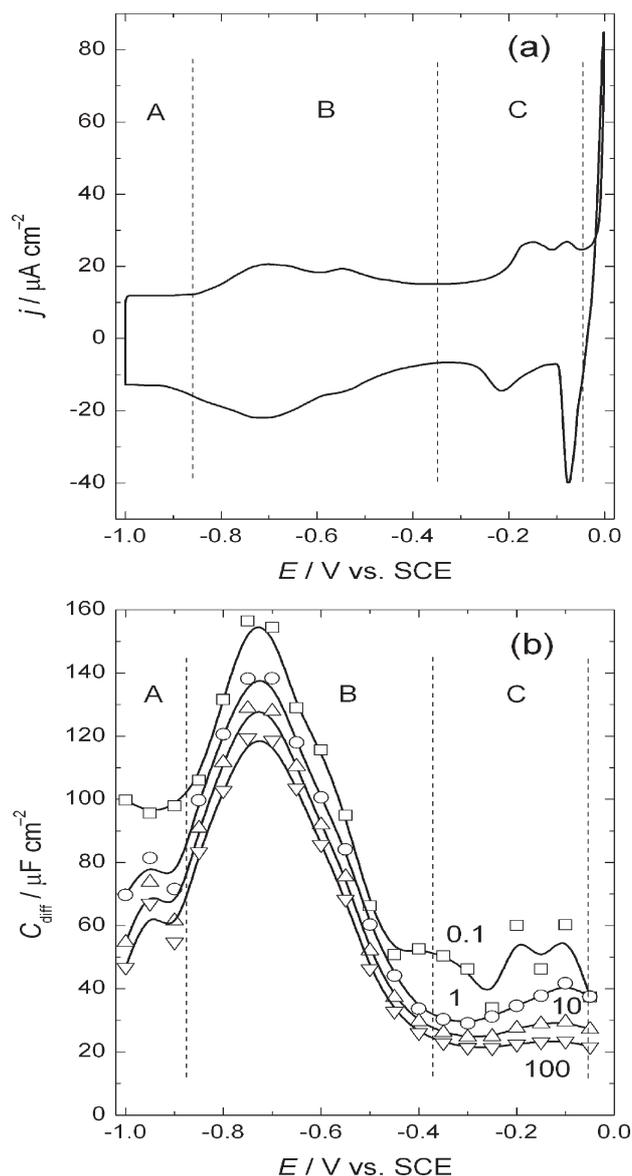
F i g . 8 – *(a) CV of Ag(poly) in 0.01 M NaBr + 0.1 M NaClO$_4$ recorded at a sweep rate of 100 mV s^{-1}. (b) Corresponding C_{diff} vs. E curves recorded at different frequencies (marked in the figure in Hz).*
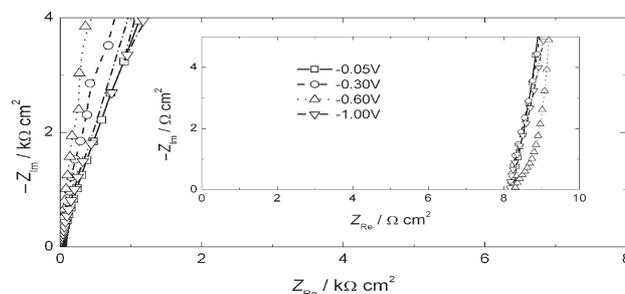
F i g . 9 – *Z_{Im} vs. Z_{Re} diagrams recorded at different potentials (marked in the figure) in the frequency range from 0.01 to 10000 Hz for the system Ag(poly)/0.01 M NaBr + 0.1 M NaClO$_4$. The high frequency ends of Z_{Im} vs. Z_{Re} diagrams, used for determination of R_s, are presented in the inset.*
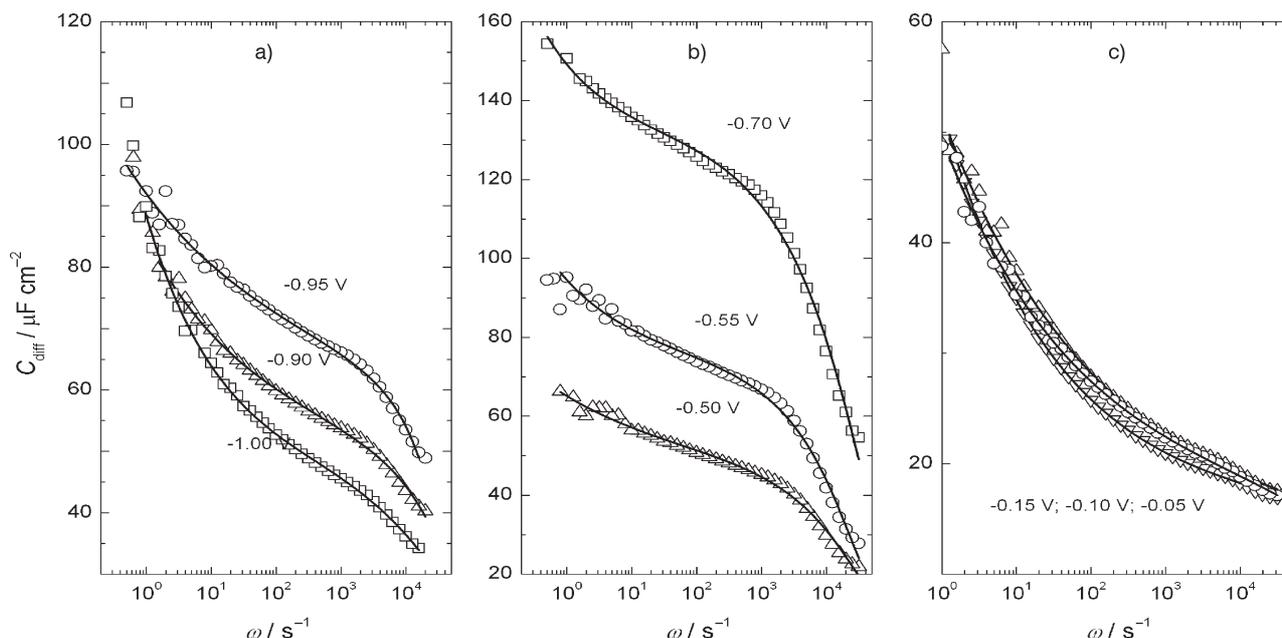
F i g . 1 0 – *C_{diff} vs. ω curves for different potentials (marked in the figure) obtained from the EIS measurements for the system Ag(poly)/0.01 M NaBr + 0.1 M NaClO$_4$. The squares, circles, triangles, etc. represent the experimental points, while the full lines represent the fitted curves obtained by using eq. (7).*

curve. Identical results were obtained for the rest of the C_{diff} vs. ω curves, not presented in Fig. 10.

The dependences of the parameters C_{dl}, C_{ad}, $(C_{dl} + C_{ad})$, R_{ad}^{ho}, R_{ad}^{he}, σ and α as a function of potential are shown in Fig. 11. From Fig. 11a it can be seen that the value of C_{dl} is practically negligible, and that $(C_{dl} + C_{ad})$ vs. E and C_{ad} vs. E curves are identical, coinciding well with the corresponding CV, whereas the value of α is much smaller in comparison with the one detected for the Ag(100) (see Fig. 7a, before the sharp peak on the CV), decreas-

ing at the maximum on the C_{ad} vs. E (△) curve. Such behavior of α indicates significant heterogeneity of the charge distribution over the electrode surface in the entire investigated potential range, as should be expected for the polycrystalline surface. Hence, in the presence of the supporting, "non-adsorbing" electrolyte, C_{dl} is practically independent of potential. The R_{ad}^{ho} vs. E and C_{ad} vs. E dependences, shown in Fig. 11b, possess the shapes expected for a serial connection of R_{ad}^{ho} and C_{ad}. Although the process of bromide anions adsorption cannot be diffusion controlled, the high value of the Warburg constant σ, shown in Fig. 11c, indicates that some diffusion-like phenomenon is involved in the process of anion adsorption.

Discussion

The bromide anions are known as strongly adsorbing species characterized by the formation of ordered adsorbate structures on all investigated single crystal faces.[48–60] It is important to note that, except in our recent papers[28,46] and papers of Kerner *et al.*[13] and Pajkossy,[12,14,15] in all previous[1–8] and later[48–56] investigations it was assumed that the double layer behaves as an "ideal double layer", neglecting the possibility of heterogeneity of the electrode surface. Different techniques were employed in these investigations: LEED-Auger,[51] in situ STM,[43,45] in situ XAFS,[52] in situ X-ray,[53,54] EIS,[55–57] differential capacity measurements,[48–50] thermodynamic analysis – chronocoulometric curves[48–50] and

F i g . 1 1 – *Results obtained by fitting the C_{diff} vs. ω curves for different potentials with eq. (7) for the system Ag(poly)/0.01 M NaBr + 0.1 M NaClO$_4$; (a) C_{ad} vs. E (△), C_{dl} vs. E (○), $(C_{dl} + C_{ad})$ vs. E (□) and α vs. E (▼) curves. (b) C_{ad} vs. E (△) and R_{ad}^{ho} vs. E (■). (c) C_{ad} vs. E (△) and σ vs. E (○) curves.*

cyclic voltammetry in all papers.[5–67] Most of the experiments were performed in the presence of the "non-adsorbing" supporting electrolyte (mainly $KClO_4$ or $HClO_4$) with the addition of a low concentration of bromide anions (up to 10 mM), while in a few of them one component (KBr, NaBr, HBr) electrolytes were used[43,51,53] respectively, and adsorption of bromide anion was investigated in the absence of the supporting electrolyte. A common feature of the experiments performed in the presence of "non-adsorbing" supporting electrolyte is the appearance of peaks on CVs for pure supporting electrolyte, corresponding to the specific adsorption of ClO_4^- anions to some extent.[48–50,55–57] Also, in all papers with differential capacity measurements, the C_{diff} vs. E curves were recorded only at one constant frequency (1 Hz or 18 Hz) at the sweep rate of 10 mV s^{-1} and 10 mV peak-to-peak amplitude. T. Wandlowski *et al.*[48] clearly stated that "differential capacity vs. potential curves do not provide equilibrium data for Br$^-$ adsorption onto Ag(100) surface in the low and medium concentration regions", with this comment being relevant to the curves recorded at one frequency only. It should also be stated here that the differential "capacity dispersion", recorded even in a pure supporting electrolyte (0.1 M $HClO_4$), as well as in the presence of adsorbing anions in a very narrow frequency range (12 Hz < f < 80 Hz), has been observed by Hamelin and coworkers on "perfect" single crystals.[5] All authors employing thermodynamic analysis[48–50] assumed that the adsorption of anions from the supporting electrolyte is negligible. It is characteristic that, in all these cases, the values of the electrosorption valence ($-\gamma$) were smaller than 1, indicating partial charge transfer during bromide anions adsorption. On the other hand, in only one paper[53] was the value of $\gamma = -1 \pm 0.2$ for bromide anions adsorption onto Au(111) obtained by the analysis of Γ vs. E curves at different anion concentrations. It is characteristic that in some papers employing EIS,[6–8,56,57] Z_{Im} vs. Z_{Re} diagrams were used for fitting experimental results with corresponding equivalent circuit for the diffusion control of anion adsorption. It is important to note here a statement of D. Eberhardt *et al.*[55] concerning the fitting procedure for such a case: "Although the resulting equivalent circuit represents very well the surface processes occurring at the interface, it should be pointed out that the employment of such a complicated combination of elements conduces to rather high correlation factor between the fitted values, so that the individual elements can be determined only with a fairly large uncertainty".

Hence, the generally accepted explanation for the frequency dependence of the interfacial – differential capacity ("capacity dispersion") could be given as: this phenomenon is a consequence of either adsorption of organic or certain inorganic species[58,59] or molecules,[60,61] or surface roughness and heterogeneity,[9–15,28,46] or specific adsorption of anions.[28,46–50,62,63] It should be emphasized here that, except in our previous papers,[28,46] the "capacity dispersion" as a consequence of both anion adsorption and surface heterogeneity, has not been considered in the literature.

This work considers both cases: adsorption of only one anion (solution of pure NaBr salt) in the absence of supporting electrolyte, and adsorption of the same anion of the same concentration in the presence of "non-adsorbing" supporting electrolyte (0.1 M $NaClO_4$ – possible competitive adsorption). At the same time, the possibility for diffusion-controlled adsorption of anions is avoided by using concentrations at which the adsorption process is under activation control.

System Ag(100)/0.01 M NaBr

As can be seen, the CV shown in Fig. 4a is in good agreement with the results of other authors.[48–50]

The shape of the impedance diagrams shown in Fig. 5 indicates deviation from the "ideal double layer" behavior.[9–15] Impedance diagram recorded at –0.3 V vs. SCE ($\triangle$) is very similar to the one that might correspond to diffusion-controlled adsorption,[7] but an attempt to fit this diagram with the corresponding equation for diffusion-controlled impedance was not possible, and this is one more argument for the statement that such a shape of the impedance diagram could be a consequence of surface heterogeneity, as well as specific anion adsorption.

The importance of the solution resistance subtraction should be emphasized here. As can be seen in the inset of Fig. 5, values of Z_{Re} at frequencies lower than 1 kHz are very close to the value of R_s and if R_s is not subtracted, lower values for C_{diff} would be obtained (see eq. (8)).

The C_{diff} vs. E curves as a function of frequency are presented in Fig. 4b. The shape of the C_{diff} vs. E curves is practically identical to the shape of CV at low frequencies (lower than 10 Hz). The influence of the frequency on the shape of this dependence is also evidence of the deviation from the "ideal double layer" behavior, while the similarity between the shape of C_{diff} vs. f curves simulated and presented in Fig. 3a and the experimentally obtained ones (C_{diff} vs. ω presented in Fig. 6) could only be ascribed to the presence of both specific adsorption of anions and the surface heterogeneity.

Comparing ($C_{dl} + C_{ad}$) vs. E curve (Fig. 7a) with C_{diff} vs. E curves (Fig. 4b), it could be con-

cluded that C_{diff} vs. E curves show higher values for the capacity than the one presented in Fig. 7a. Hence, it seems that neither of the curves presented in Fig. 4b could be considered relevant for the system Ag(100)/0.01 M NaBr. Only after fitting C_{diff} vs. ω curves recorded at different potentials was the correct differential capacity vs. potential curve, $(C_{dl} + C_{ad})$ vs. E obtained.

Considering the results presented in Fig. 7a, it could be concluded that the shape of the C_{ad} vs. E curve is much more similar to the shape of CV than the other two curves. Fig. 7a illustrates that C_{dl} increases with potential up to –0.75 V and then sharply decreases to the very small values of about 3–5 μF cm^{-2}. At the position of a maximum on the C_{ad} vs. E curve, C_{dl} is practically negligible and at potentials more positive than –0.60 V a total capacity $(C_{dl} + C_{ad})$ is practically determined by the value of C_{ad}. The value of α sharply decreases from about 0.95 at –0.70 V to about 0.45 at –0.10 V. This system has already been analyzed by Wandlowski *et al.*[48] and it was shown by SXS analysis that with increasing electrode potential, bromide undergoes a phase transition from a lattice gas to an ordered $c(2 \times 2)$ structure, and that this structure is formed at the potential of the sharp peak on both the CV and C_{diff} vs. E curves. Taking into account that, in the case of bromide adsorption, incommensurate adsorbed structures, compressing uniformly with increasing potential, have been detected[53–55] after the commensurate ordered structures were formed (sharp peak on the CV), such a change of the surface homogeneity, i.e. the change of α, could be expected. At the same time, it is important to note that at potentials close to 0.0 V vs. SCE a "nucleation loop" can be detected (not shown in this figure), indicating the formation of 3D layer (see Fig. 8a) of AgBr (similar to behavior of Ag(111) in 0.1 M NaCl[64]). It is quite reasonable to assume that the transformation of ordered $c(2 \times 2)$ adsorbed structure into 3D layer should be accompanied by the change of the charge distribution, i.e. the homogeneity of the electrode surface.

Concerning the R_{ad}^{ho} vs. E and R_{ad}^{he} vs. E curves it is seen that the values of R_{ad}^{ho} and R_{ad}^{he} are of the same order of magnitude, varying between 0.1 and 4.5 kΩ cm^2 (Fig. 7b). At the beginning of the adsorption process, the R_{ad}^{ho} is high, whereas R_{ad}^{he} is low, indicating faster adsorption of bromide anions at the monoatomic steps. In the region of sharp peaks on C_{ad} vs. E curve, R_{ad}^{ho} sharply decreases, while R_{ad}^{he} sharply increases, as it could be expected. It is important to note that in this case the shapes of C_{ad} vs. E and R_{ad}^{ho} vs. E curves are far from being a mirror-image of one another.[28] Such a behavior is most likely the consequence of the formation of incommensurate adsorbed structures at

potentials more positive than the potential of sharp peak on the CV,[53–55] i.e. a sharp decrease of surface homogeneity (decrease of α).

Finally, considering charges presented in Table 1, it could be concluded that the charge under the anodic part of the CV is higher than that obtained by integration of $(C_{dl} + C_{ad})$ vs. E curve. At the same time, charges corresponding to the C_{ad} vs. E and C_{dl} vs. E curves are almost identical. Taking into account that for a formation of ordered $c(2 \times 2)$ structure the theoretical charge needed (assuming complete charge transfer) amounts to 96 μC cm^{-2}, it appears that for the formation of this structure $\gamma = -0.32$ (31 μC cm^{-2} over 96 μC cm^{-2}). Hence, this analysis clearly indicates that neither the charge under the CV, nor that under C_{diff} vs. E curve recorded at a single frequency and C_{ad} vs. E and C_{dl} vs. E curves, can be considered relevant for determining either the structure of adsorbed anions or the value of γ. At the same time, in order to define correct charges corresponding to the adsorption on the heterogeneous and the homogeneous part of the surface (as well as correct values of C_{dl} and C_{ad}) it is necessary to know exactly the corresponding surface area (on the atomic level), which is practically impossible using present techniques for the surface characterization.

System Ag(poly)/0.01 M NaBr + 0.1 M NaClO$_4$

In the case of polycrystalline surface, sharp peaks for ordered adsorbed structures cannot be expected, as can be seen on the CV shown in Fig. 8a. Comparing CVs recorded for single crystal surfaces[48–60,65] one can conclude that in the region (B) adsorption on the heterogeneous part of the surface takes place, while, most probably, ordered structures are formed in the region (C). The "nucleation loop" at potential close to 0.0 V vs. SCE is a consequence of the formation of 3D layer of AgBr.[64] A similar conclusion can be drawn from the shape of the C_{diff} vs. E curves, shown in Fig. 8b.

The EIS results (Fig. 9) clearly show deviation from the "ideal double layer" behavior at all investigated potentials, as well as much lower value of R_s in the presence of the supporting electrolyte (inset of Fig. 9) in comparison with the one recorded for the system Ag(100)/0.01 M NaBr. Although the solution resistance is much smaller in the presence of 0.1 M NaClO$_4$, the importance of its subtraction is as significant as in the system Ag(100)/0.01 M NaBr, since at high frequencies Z_{Re} values are also very close to the value of R_s and the precision of the R_s determination is very important.

A very good fit of the experimentally recorded C_{diff} vs. ω curves (Fig. 10) clearly indicates that for this system eq. (7) must be used. Resulting values

of adsorption parameters, presented in Fig. 11 as a function of potential, confirm that in the presence of 0.1 M NaClO$_4$ different dependences were obtained in comparison with those recorded in a pure NaBr salt. The ($C_{dl} + C_{ad}$) vs. *E* curve is practically identical to the C_{ad} vs. *E* curve, while the value of C_{dl} is almost independent of potential and much smaller than expected for the "ideal double layer capacity" ($C_{dl} = 20$ μF cm^{-2}, Fig. 11a). At the same time, as it might be expected, charge distribution over the polycrystalline surface is heterogeneous, reaching maximum value of $\alpha = 0.8$ (Fig. 11a). Considering the shapes of C_{ad} vs. *E* and R_{ad}^{ho} vs. *E* curves, one can conclude that they are more or less a mirror-image of one another[28] (Fig. 11b). The most interesting is σ vs. *E* dependence. Taking into account that the constant σ represents the presence of Warburg-like impedance and that the diffusion of anions from the bulk of solution is excluded at such anion concentration, it seems most likely that the diffusion phenomenon is connected with the replacement and exchange of anions in the inner Helmholtz plane. Actually, ClO$_4^-$ anions are already adsorbed on the electrode surface when Br$^-$ anions start to adsorb. Since the adsorption of Br$^-$ anions is much stronger, ClO$_4^-$ anions must be desorbed and replaced with bromides. This process is obviously slow step in the overall reaction, being expressed as the diffusion-like phenomenon, and accordingly eq. (7) must be used to fit experimentally recorded C_{diff} vs. ω curves (Fig. 10). According to the results presented in Fig. 11c, this effect is more pronounced in the region of ordered (more dense) adsorbed structure formation (potential region C), where all ClO$_4^-$ anions must be removed and replaced with bromides. It is most likely that removed ClO$_4^-$ anions again adsorb on the bromide layer, as it was the case in UPD of Cd onto Cu(111)[66] and Cd onto Ag(111) in the presence of chloride anions.[67] A similar effect has recently been recognized by T. Pajkossy and D. M. Kolb[68] in the double layer region of Pt(111) and Ir(111) in the presence of only one anion (much simpler case) and they attributed the frequency dependence of the interfacial capacitance to the relatively slow exchange of anions between the outer and inner Helmholtz planes. At this moment a convincing explanation for the observed phenomenon is missing and it will be the subject of further investigations.

Conclusion

For the determination of the adsorption parameters, a new equivalent circuit and corresponding equation for analyzing anion adsorption, based on a different definition of the constant phase element, has been developed and used in this work. It is shown that such analysis can successfully be applied in the case of bromide anions adsorption in two systems: Ag(100)/0.01 M NaBr and Ag(poly)/0.01 M NaBr + 0.1 M NaClO$_4$. Homogeneity of the charge distribution over the electrode surface was found to change as a consequence of the adsorption of bromide anions in both cases. It was shown that in the presence of the supporting electrolyte (0.1 M NaClO$_4$) Warburg impedance must be introduced in the equivalent circuit (and corresponding equation for C_{diff}) in order to fit experimentally recorded C_{diff} vs. ω curves. This phenomenon was explained by the slow step of replacement of already adsorbed perchlorate anions with bromide anions.

Symbols

C	–	capacitance, F cm^{-2}
c	–	concentration of adsorbing anions, M
C_{ad}	–	adsorption capacitance, μF cm^{-2}
C_{diff}	–	differential capacitance, μF cm^{-2}
C_{dl}	–	double layer capacitance, μF cm^{-2}
CPE	–	constant phase element
CPE_{dl}^{he}	–	constant phase element of the heterogeneous part of the surface
D	–	diffusion coefficient of adsorbing anions, cm^2 s^{-1}
f	–	frequency, Hz
R	–	resistance, Ω cm^2
R_{ad}	–	adsorption resistance, Ω cm^2
R_{ad}^{he}	–	adsorption resistance on the heterogeneous part of the surface, Ω cm^2
R_{ad}^{ho}	–	adsorption resistance on the homogeneous part of the surface, Ω cm^2
R_s	–	solution resistance, Ω cm^2
Y_{Im}	–	imaginary component of admittance, Ω^{-1} cm^{-2}
Y_0	–	constant, Ω^{-1} cm^{-2} s$^\alpha$
Z_{Re}	–	real component of impedance, Ω cm^2
Z_{Im}	–	imaginary component of impedance, Ω cm^2
Z_{CPE}	–	impedance of the CPE
α	–	factor of the charge distribution homogeneity
σ	–	Warburg coefficient, Ω cm^2 s$^{-1/2}$
ω	–	angular frequency, s^{-1}

References

1. *Reeves, R.,* The Double Layer in the Absence of Specific Adsorption, in *Bockris, J. O'M. Conway, B. E.,* and *Yeager, E.* (Eds.), Comprehensive Treatise of Electrochemistry, Vol. 1, Plenum, New York and London, 1980, pp. 83–132.
2. *Valette, G., Hamelin, A.,* J. Electroanal. Chem. **45** (1973) 301.
3. *Gouy, G.,* J. Phys. **9** (1910) 457.
4. *Gouy, G.,* C. R. Acad. Sci. **149** (1910) 654.

5. *Hamelin, A.,* Double-layer properties at *sp* and *sd* metal single-crystal electrodes, in *Conway, B. E., White, R., Bockris, J. O'M.* (Eds.), Modern Aspects of Electrochemistry, Vol. 16, Plenum, New York, 1985, pp. 1–98.

6. *El-Aziz, A. M., Kibler, L. A., Kolb, D. M.,* Electrochem. Comm. **4** (2002) 535.

7. *Sluyters-Rehbach, M., Sluyters, J.,* Sine Wave Methods in the Study of Electrode Processes, in *Bard, A.* (Ed.), Electroanalytical Chemistry, Vol. 4, Marcel Dekker, New York, 1970, pp. 75–80.

8. *Kerner, Z., Pajkossy, T., Kibler, L. A., Kolb, D. M.,* Electrochem. Comm. **4** (2002) 787.

9. *Sluyters-Rehbach, M.,* Pure & Appl. Chem. **66** (1994) 1831.

10. *Nyikos, L., Pajkossy, T.,* Electrochim. Acta **35** (1990) 1567.

11. *Mandelbrot, B. B.,* The Fractal Geometry of Nature, Freeman, San Francisco, 1982.

12. *Pajkossy, T.,* Solid State Ionics **94** (1997) 123.

13. *Kerner, Z., Pajkossy, T.,* Electrochim. Acta **46** (2000) 207.

14. *Pajkossy, T.,* Heterogeneous Chem. Rev. **2** (1995) 143.

15. *Pajkossy, T.,* J. Electroanal. Chem. **364** (1994) 111.

16. *Motheo, A. J., Sadkowski, A., Neves, R. S.,* J. Electroanal. Chem. **430** (1997) 253.

17. *Zoltowski, P.,* J. Electroanal. Chem. **443** (1998) 149.

18. *Sadkowski, A., Motheo, A. J., Neves, R. S.,* J. Electroanal. Chem. **445** (1998) 107.

19. *Láng, G., Heusler, K. E.,* J. Electroanal. Chem. **457** (1998) 257.

20. *Zoltowski, P.,* J. Electroanal. Chem. **481** (2000) 230.

21. *Sadkowski, A.,* J. Electroanal. Chem. **481** (2000) 232.

22. *Láng, G., Heusler, K. E.,* J. Electroanal. Chem. **481** (2000) 227.

23. *Sadkowski, A.,* J. Electroanal. Chem. **481** (2000) 222.

24. *Jorcin, J.-B., Orazem, M. E., Pébčre, N., Tribollet, B.,* Electrochim. Acta **51** (2006) 1473.

25. *Kerner, Z., Pajkossy, T.,* J. Electroanal. Chem. **448** (1998) 139.

26. *Kim, C.-H., Pyun, S.-I., Kim, J. H.,* Electrochim. Acta **48** (2003) 345.

27. *Orazem, M. E., Shukla, P., Membrino, M. A.,* Electrochim. Acta **47** (2002) 2027.

28. *Jović, V. D., Jović, B. M.,* J. Electroanal. Chem. **541** (2003) 1.

29. *Macdonald, J. R.,* Impedance Spectroscopy Emphasizing Solid Materials and Systems, Wiley, New York, Chichester, Brisbane, Toronto, Singapore, 1987.

30. *Brug, G. J., Van Eeden, A. L. G., Sluyters-Rehbach, M., Sluyters, J.,* J. Electroanal. Chem. **176** (1984) 275.

31. *Hsu, C. H., Mansfeld, F.,* Corrosion **57** (2001) 747.

32. *Van Meirhaeghe, R. L., Dutiot, E. C., Cardon, F., Gomes, W. P.,* Electrochim. Acta **20** (1975) 995.

33. *Morrison, S. R.,* Electrochemistry at Semiconductor and Oxidized Metal Electrodes, Plenum Press, New York, 1980.

34. *Moffat, T. P.,* Scanning tunneling microscopy studies of metal electrodes, in *Bard, A. J., Rubinstein, I.* (Eds.), Electroanalytical Chemistry: a Series of Advances, Vol. 21, Marcel Dekker Inc., New York, Basel, 1999, pp. 211–316.

35. *Schweizer, M., Kolb, D. M.,* Surf. Sci. **544** (2003) 93.

36. *Garcia, S. G., Salinas, D. R., Mayer, C. E., Lorenz, W. J., Staikov, G.,* Electrochim. Acta **48** (2003) 1279.

37. *Kunze, J., Streblow, H.-H., Staikov, G.,* Electrochem. Comm. **6** (2004) 132.

38. *Wilms, M., Broekmann, P., Kruft, M., Park, Z., Stuhlmann, C., Wandelt, K.,* Surf. Sci. **402–404** (1998) 83.

39. *Wan, L., Suzuki, T., Sashikata, K., Okada, J., Inutai, J., Itaya, K.,* J. Electroanal. Chem. **484** (2000) 189.

40. *Maurice, V., Streblow, H.-H., Marcus, P.,* Surf. Sci. **458** (2000) 185.

41. *Kunze, J., Maurice, V., Klein, L. H., Streblow, H.-H., Marcus, P.,* J. Phys. Chem. B **105** (2001) 4263.

42. *Streblow, H.-H., Maurice, V., Marcus, P.,* Electrochim. Acta **46** (2001) 3755.

43. *Broekmann, P., Anastesescu, M., Spaenig, A., Lisowski, W., Wandelt, K.,* J. Electroanal. Chem. **500** (2001) 241.

44. *Li, W. H., Wang, Y., Ye, J. H., Li, S. F. Y.,* J. Phys. Chem. B **105** (2001) 1829.

45. *Cuesta, A., Kolb, D. M.,* Surf. Sci. **465** (2000) 310.

46. *Jović, V. D., Jović, B. M.,* J. Electroanal. Chem. **541** (2003) 12.

47. *Jovićević, J. N., Jović, V. D., Despić, A. R.,* Electrochim. Acta **29** (1984) 1625.

48. *Wandlowski, Th., Wang, J. X., Ocko, B. M.,* J. Electroanal. Chem. **500** (2001) 418.

49. *Hamad, I. A., Wandlowski, T., Brown, G., Rikvold, P. A.,* J. Electroanal. Chem. **554–555** (2003) 211.

50. *Beltramo, G., Santos, E.,* J. Electroanal. Chem. **556** (2003) 127.

51. *Reniers, F., Fairbrother, D.-H., Wu, S., Lipkowski, J.,* Surf. Sci. **433–435** (1999) 12.

52. *Endo, O., Matsumura, D., Kohdate, K., Kiguchi, M., Yokoyama, T., Ohta, T.,* J. Electroanal. Chem. **494** (2000) 121.

53. *Magnussen, O., Ocko, B. M., Adžić, R. R., Wang, J. X.,* Phys. Rev. B **51** (1995) 5510.

54. *Magnussen, O., Ocko, B. M., Wang, J. X., Adžić, R. R.,* J. Phys. Chem. B **100** (1996) 5500.

55. *Eberhardt, D., Santos, E., Schmickler, W.,* J. Electroanal. Chem. **419** (1996) 23.

56. *Pajkossy, T., Wandlowski, T., Kolb, D. M.,* J. Electroanal. Chem. **414** (1996) 209.

57. *Kerner, Z., Pajkossy, T.,* Electrochim. Acta **47** (2002) 2055.

58. *Lorenz, W., Möckel, F.,* Z. Elektrochem. **60** (1994) 507.

59. *Armstrong, R. D., Rice, W. C., Thirsk, H. R.,* J. Electroanal. Chem. **16** (1968) 517.

60. *Van Houng, C. N., Hinnen, C., Dalbera, J. P., Parsons, R.,* J. Electroanal. Chem. **125** (1981) 177.

61. *Lipkowski, J., Van Houng, C. N., Hinnen, C., Parsons, R., Chevalet, J.,* J. Electroanal. Chem. **143** (1983) 375.

62. *Jović, V. D., Jović, B. M., Parsons, R.,* J. Electroanal. Chem. **290** (1990) 257.

63. *Jović, V. D., Parsons, R., Jović, B. M.,* J. Electroanal. Chem. **339** (1992) 327.

64. *Jović, B. M., Jović, V. D., Dražić, D. M.,* J. Electroanal. Chem. **399** (1995) 197.

65. *Jović, B. M., Dražić, D. M., Jović, V. D.,* J. Serb. Chem. Soc. **64** (1999) 47.

66. *Stulmann, C., Park, Z., Bach, C., Wandelt, K.,* Electrochim. Acta **44** (1998) 993.

67. *Jović, V. D., Jović, B. M.,* Electrochim. Acta **47** (2002) 1777.

68. *Pajkossy, T., Kolb, D. M.,* Electrochem. Comm. **9** (2007) 1171.